Shear Properties of Acrylic Under High Strain Rate Loading

Tamrat Abishu Gelu,[1] S. S. Joshi,[1] N. K. Naik[2]

[1]*Mechanical Engineering Department, Indian Institute of Technology Bombay, Powai, Mumbai 400076, India*
[2]*Aerospace Engineering Department, Indian Institute of Technology Bombay, Powai, Mumbai 400076, India*

Received 9 August 2010; accepted 10 November 2010
DOI 10.1002/app.33719
Published online 4 March 2011 in Wiley Online Library (wileyonlinelibrary.com).

ABSTRACT: Acrylic is being used in structural applications because of its higher resistance to projectile impacts. High strain rate shear loading is one of the critical conditions. In the present study, properties of typical acrylic under high strain rate shear loading are presented. Torsional Split Hopkinson Bar apparatus was used for the studies in the shear strain rate range of 290 per sec to 791 per sec. Thin-walled tubular specimens with hexagonal flanges were used for the experimental studies. Details of specimen configuration, data acquisition, and processing are presented. Shear strength is presented as a function of shear strain rate. It is observed that the shear strength at high strain rate is enhanced up to 25% compared with that at quasi-static loading in the range of parameters considered. Comparison of torque versus time behavior derived from signals obtained from strain gauges mounted on incident bar and transmitter bar is also presented. © 2011 Wiley Periodicals, Inc. J Appl Polym Sci 121: 1631–1639, 2011

Key words: acrylic; mechanical properties; shear; stress; strain; strength

INTRODUCTION

Acrylic is being used in structural applications in the areas of aerospace, car manufacturing, as well as in making composite materials subjected to dynamic loading. A research study by Rosenberg et al.[1] has shown that Plexiglas, which is one form of acrylic, has a fascinating resistance to projectile impacts if it is used as an oblique target. The mechanical properties of polymeric materials and their composites under quasi-static loading conditions are well known. But there are limited studies in literatures on high strain rate shear behavior of polymers. The objective of the present study is to investigate high strain rate behavior of acrylic under shear loading.

High strain rate shear behavior of materials can be studied using different testing techniques.[2] These include drop weight impact test, pressure-shear plate impact test, and Hopkinson bar test. The Hopkinson bar testing technique is the most widely used method to study the shear behavior of materials at high strain rates. Thin walled tubular specimens are used in Torsional Split Hopkinson Bar (TSHB) testing, whereas single-lap and double-lap shear specimens are used in Split Hopkinson Pressure Bar (SHPB) testing to characterize the shear behavior of materials.

Sayers and Harris[3] determined the interlaminar shear properties of carbon/epoxy composites using drop weight impact test technique. Werner and Dharan[4] used compressive SHPB apparatus to perform interlaminar shear experiments on woven graphite/epoxy. They used short-beam shear specimen.

Harding and coworkers[5,6] carried out both experimental as well as numerical analysis on the interlaminar shear strength of plain weave carbon/epoxy and plain weave glass/epoxy composites. They used double-lap specimens. They observed an increase in the mean value of interlaminar shear strength with increasing strain rate in both the materials.

Single-lap specimens were used for determining the interlaminar shear properties of composites.[7–10] The major advantage of single-lap specimen is that the central interlaminar plane is on the axis of the externally applied loading.

For shear characterization of materials under high strain rate loading, torsional tests are the most accurate test techniques. Typical studies based on the torsional tests are presented in Refs. 11–13. In these studies, short circular thin walled tubular specimens were used. These studies were on metallic specimens. Modified geometry of the specimen was used for interlaminar shear properties of composites by Leber and Lifshitz.[14] The studies were carried out on interlaminar shear behavior of plain weave E-glass/

Correspondence to: N. K. Naik (nknaik@aero.iitb.ac.in).

Figure 1 Photograph of TSHB apparatus. [Color figure can be viewed in the online issue, which is available at wileyonlinelibrary.com.]

epoxy laminate at static and high strain rate shear loading. High aspect ratio thin walled circular specimens were used for their experiments. The experiments were performed at shear strain rate range of 300–500 per second on TSHB apparatus. They reported that there is about 50% increase of dynamic fracture stress, about 60% increase of initial shear modulus, and ~25% enhancement of strain to failure.

They also studied response of plain weave E-glass/epoxy and unidirectional carbon fiber/epoxy to high strain rate loading in interlaminar tension and combined tension/shear.[15] Interlaminar shear strength (ILSS) of plain weave S2-glass/SC 79 composites subjected to high strain rate out-of-plane compressive loading was reported by Gillespie et al.[16] The studies were performed on SHPB apparatus at strain rate up to 1000 per second. They observed that ILSS was strain rate sensitive for these material systems.

Dai et al.[17,18] used TSHB apparatus for their studies. Their studies were on unidirectional C_f/A356.0 metal matrix composite and A356.0 aluminum alloy. The fibers were aligned with the direction of torsional axis. They observed multi-stage failure process and a multi-scale zigzag fracture at all the surfaces. Their studies indicated that the carbon fibers did not improve the shear strength of aluminum matrix.

Fleck et al.[19] studied high strain rate shear response of polycarbonate (PC) and polymethyl methacrylate (PMMA) using TSHB apparatus at different shear strain rates and temperatures. They conducted the experiments in the shear strain rate range of 500–2200 per second and, temperature range of -100–200°C.

Failure mechanism of unidirectional carbon-fiber epoxy laminates due to combined compression and torsion loading at quasi-static rate was studied by Jelf and Fleck.[20] The transient large-strain response of polymer melts at high shear rates using TSHB was studied by Hu and Feng.[21] They carried out the experiment on a molten low-density polyethylene in the strain rate range of 800–9900 per second and temperature range of 150–210°C.

Gilat et al.[22–24] used thin-walled tubular specimens to study the strain rate sensitivity of E-862 and PR-520 resins in tensile and shear loading in the shear strain rate range of 450–700 per second. They observed that, for both the resins, the maximum shear stress increased with increasing shear strain rate. Further, they reported that the results of their experiments were independent of wall thickness of the specimen for both the resins.

Hou et al.[25] studied the effect of strain rate on the shear properties of three different epoxies: Ciba CT200, 3*M*-PR500, and Cytec 5250-4. Experiments were performed at quasi-static and high strain rates.

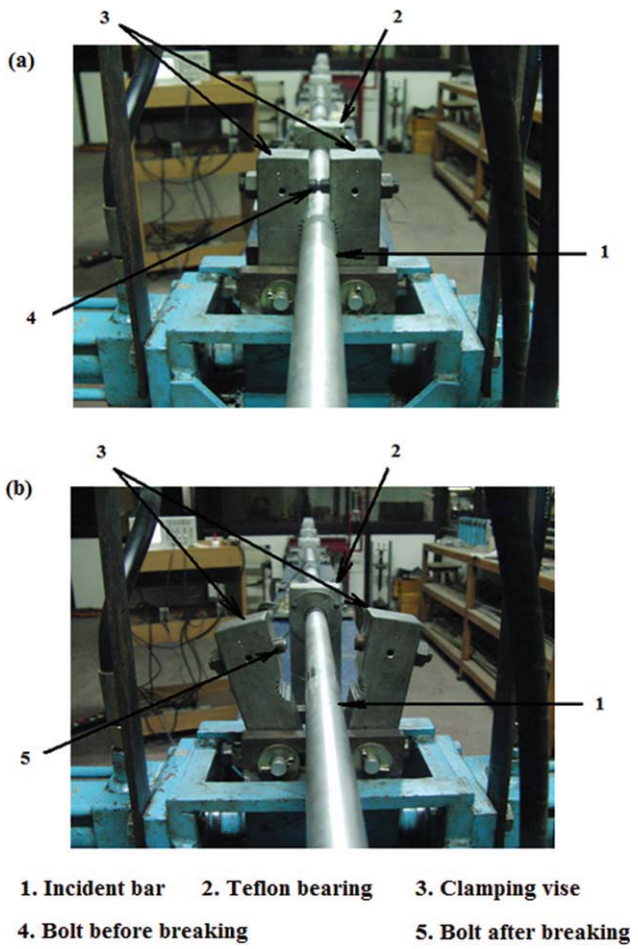

Figure 2 Photograph of clamping mechanism: (a) before breaking the clamping bolt, (b) after breaking the clamping bolt. [Color figure can be viewed in the online issue, which is available at wileyonlinelibrary.com.]

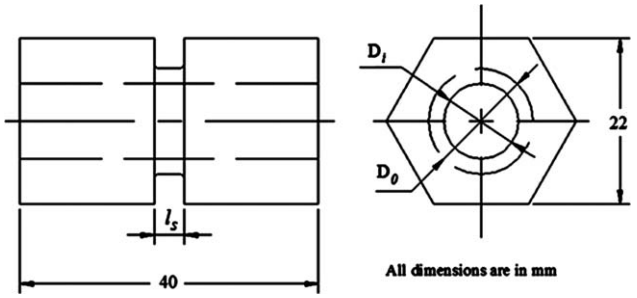

Figure 3 Schematic arrangement of thin-walled tubular specimen with hexagonal flanges used for TSHB experiments.

High strain rate tests were carried out in the strain rate range of 1000–2300 per second on TSHB apparatus. Peak stress in the range of 90–100 MPa was recorded.

Naik et al.[26] reported the interlaminar shear properties of two typical polymer matrix composites at high strain rate loading. They carried out the experiments on TSHB apparatus at shear strain rate range of 496–1000 per second. Their study on plain weave carbon/epoxy and plain weave E-glass/epoxy composites showed that interlaminar shear strengths of both the materials increased with increasing shear strain rate. They also observed that interlaminar shear properties of both the materials are nearly the same.

Naik et al.[27] used TSHP apparatus to study the effects of shear strain rate on epoxy resin LY 556 with hardener HY 951. Circular thin-walled tubular specimens with dimensions of 2 mm wall thickness, 10 mm internal diameter, 3.5 gauge length, and 7.7 mm overall length was used for the experiment. The study was carried out in the shear strain rate range of 385–880 per second. They observed that the shear properties of the specimen changed marginally with the change in shear strain rate. But comparing the shear properties at high strain rate with those at quasi-static rate, the shear strength and shear modulus enhanced significantly while the ultimate shear strain reduced at higher strain rates.

Jacob et al.[28] presented summary of strain rate effects on the mechanical properties of polymer composite materials. As can be seen there are limited studies on the high strain rate shear behavior of polymeric materials. In the present work, high strain rate behavior of acrylic under shear loading is presented.

THEORY

The stress–strain plots under high strain rate shear loading for the specimens can be obtained by the analysis of shear stress waves in the elastic bars placed on either side of the specimen. Shear stress wave signals are obtained using the strain gauges. The portion of the incident wave that is transmitted through the specimen provides a measure of the shear stress in the specimen, while the remaining portion of the incident wave that is reflected provides a measure of strain rate and strain.[13,19,29]

The shear strain rate in the specimen is given by

$$\dot{\gamma}_S(t) = \frac{2CD_S}{L_S D}\gamma_R(t) \tag{1}$$

The shear strain in the specimen is given by

$$\gamma_S(t) = \frac{2CD_S}{L_S D}\int_0^t \gamma_R(t)\,dt \tag{2}$$

The shear stress in the specimen is give by

$$\tau_S(t) = \frac{GD^3}{8D_S^2 t_S}\gamma_T(t) \tag{3}$$

where C is torsional wave velocity in the bars, D is diameter of the bars, D_S is mean diameter of the specimen, L_S is specimen gauge length, t_S is tubular specimen wall thickness, G *is* shear modulus of the bars, γ_T is transmitted shear strain pulse and γ_R is reflected shear strain pulse.

EXPERIMENTS

The photograph of the TSHB apparatus used for the studies is presented in Figure 1. The construction and working of TSHB apparatus is presented in Appendix A. Clamping mechanism is an important component of the TSHB apparatus. Photograph of the clamping mechanism is shown in Figure 2. Thin-walled tubular specimen with hexagonal flanges as shown in Figure 3 was used for the studies. The

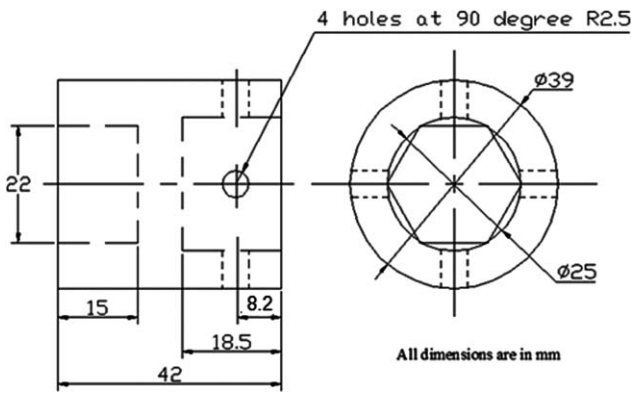

Figure 4 Aluminum specimen holder used for attaching thin-walled tubular specimens with hexagonal flanges to the elastic bars.

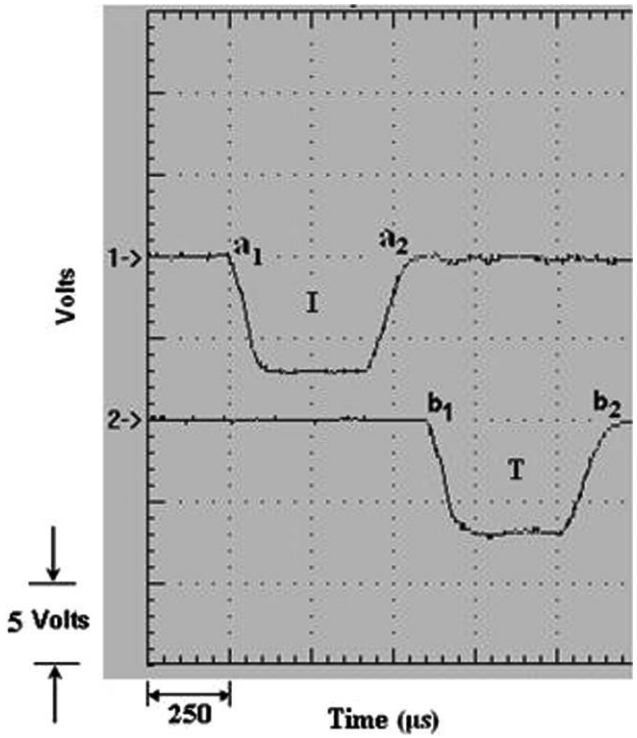

Figure 5 Strain gauge signals on oscilloscope obtained during calibration on TSHB apparatus.

specimens were mounted on the elastic bars using a specially designed aluminum specimen holders. Schematic arrangement of the holders is shown in Figure 4. Calibration of the TSHB apparatus was done before starting the experiments. Strain gauge signals on oscilloscope obtained during calibration on TSHB apparatus are shown in Figure 5. Comparison of torque versus time behavior derived from strain gauge signals during calibration on TSHB apparatus is presented in Figure 6. Details about calibration are presented in Appendix B.

Specimen geometry

Generally, thin-walled tubular specimens are used for TSHB experiments. The specimen is bonded to the incident and transmitter elastic bars. Even though this technique works well generally, there can be bonding issues especially for brittle materials.

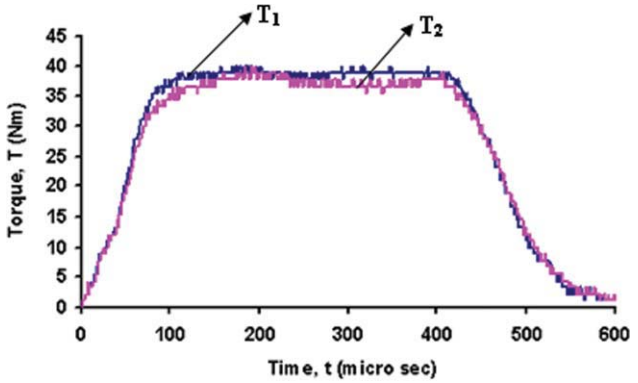

Figure 6 Comparison of torque versus time behavior, derived from strain gauge signals obtained during calibration on TSHB apparatus. [Color figure can be viewed in the online issue, which is available at wileyonlinelibrary.com.]

Another possibility is using thin-walled tubular specimens with hexagonal flanges (Fig. 3). Such specimens are attached to the elastic bars using specially designed aluminum holders (Fig. 4).

In the present study thin-walled tubular specimens with hexagonal flanges are used. Such specimens can be divided into two parts. One is the central circular thin-walled tubular part and the other is two hexagonal flanges on either side of the central circular thin-walled tubular part. The central thin-walled tubular part and the hexagonal flanges are integral with each other. Similar specimen configuration was used by Marchand and Duffy,[30] Cepus et al.,[31] and Bassim and Panic[32] for their studies on high strain rate shear behavior of metals. With the proper alignment and fitting of the specimen, holders and elastic bars, this arrangement works very well. There are no bonding issues. For the present study, the specimens were made using acrylic with wall thickness (t_s) of 1, 1.5, 2, and 3 mm, gauge length (L_s) of 1.5, 2, and 4 mm, internal diameter (D_i) of 10 mm and overall length of 40 mm. Initial studies were carried out with different combinations of wall thickness and gauge length as shown in Table I. it was observed that specimen configurations 2 and 3 work well. For specimen configuration 1, some of the specimens had premature failure during testing. This is possibly because of lower wall

TABLE I
Shear Strength of Acrylic Obtained at Different Shear Strain Rates Using Different Specimen Configurations

Specimen configuration	Wall thickness, t_s (mm)	Gauge length, l_s (mm)	Strain rate, $\dot{\gamma}$ (per sec)	Shear strength, S (MPa)
1	1.5	2	606	31
2	2	1.5	712	30
3	2	2	553	31
4	2	4	326	28
5	3	4	Specimen not failed	

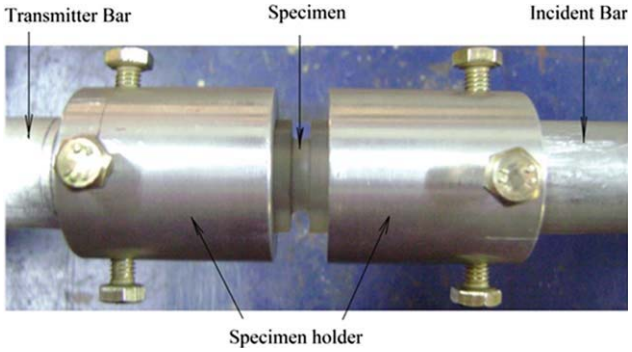

Figure 7 Photograph of a typical thin-walled tubular specimen with hexagonal flanges mounted on TSHB apparatus. [Color figure can be viewed in the online issue, which is available at wileyonlinelibrary.com.]

thickness. The effect of possible manufacturing errors would be more with lower wall thickness. With higher wall thickness, the specimen may not fail during testing. Hence, the optimum wall thickness of 2 mm and gauge length of 1.5–2.0 mm is recommended for the specimens.

The holders are designed in such a way that on one side they have hexagonal grove into which the specimen is inserted and on the other side they have circular grove through which they are fitted on to the bars. On each holder there are four holes at 90° which are diametrically arranged around the circular groove. After the holders are fitted on to the bars, they are attached to the bars using the screws through the holes. This prevents slippage between the holders and the bars when the torsional load is applied. Specimens with hexagonal flanges are inserted in to the hexagonal grooves of the holders.

Testing method

High strain rate shear studies were carried out on the TSHB apparatus as shown in Figure 1. Photograph of a typical thin-walled tubular specimen with hexagonal flanges mounted on TSHB apparatus is shown in Figure 7. The incident and transmitter bars, specimen holders, screws used for clamping the specimen holders to the bars and thin-walled tubular specimen with hexagonal flanges can be seen in the figure. In the present study, shear strain rate was varied in the range of 290–791 per sec. Details regarding control of shear strain rate and pulse duration during testing are given in Ref. 27.

As the stored torque is released instantaneously by breaking the notched clamping bolt, the part of the incident bar between the clamp and the rotary actuator where the torque was stored gets unloaded whereas the remaining part of the incident bar, specimen, and the transmitter bar get loaded.

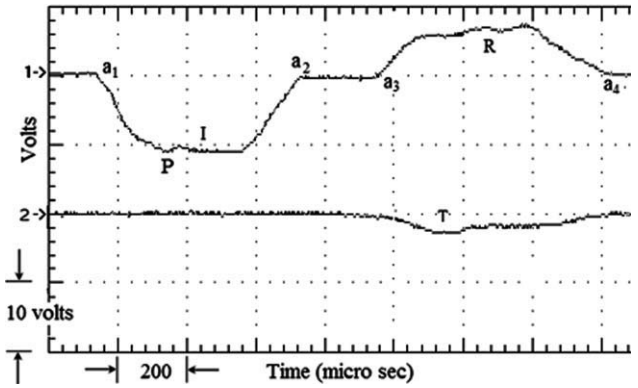

Figure 8 Strain gauge signals on oscilloscope obtained during shear test on TSHB apparatus, acrylic, $t_s = 2\ mm$, $l_s = 2\ mm$, $\dot{\gamma} = 553$ per sec.

Data processing

A typical oscilloscope plot for acrylic under high strain rate torsional loading is shown in Figure 8. Channel 1 shows the output of the strain gauge mounted on the incident bar whereas Channel 2 indicates the output of the strain gauge mounted on the transmitter bar. The plot shows incident (I), reflected (R), and transmitted (T) pulses. Point P indicates end of rise time. Using the shear wave pulses and the expressions given in theory section, shear strain rate, shear strain, and shear stress are derived as a function of time. From this, shear stress–shear strain plots are obtained.

RESULTS AND DISCUSSION

Figure 8 presents a typical oscilloscope plot for acrylic under high strain rate torsional loading. The duration of incident pulse, $a_1a_2 = 570\ \mu\ s^{-1}$. Figure 9 presents comparison of torque versus time behavior derived from strain gauge signals obtained during testing. Peak torque T_1 is more than peak torque T_2. From Figure 9, it can be observed that peak torque T_1 is attained at a time interval of 186 $\mu\ s^{-1}$. During this period, micro damage initiation and propagation

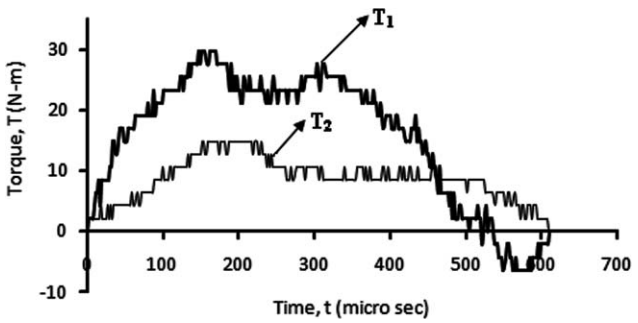

Figure 9 Comparison of torque versus time behavior, derived from strain gauge signals, acrylic, $t_s = 2\ mm$, $l_s = 2\ mm$, $\dot{\gamma} = 553$ per sec.

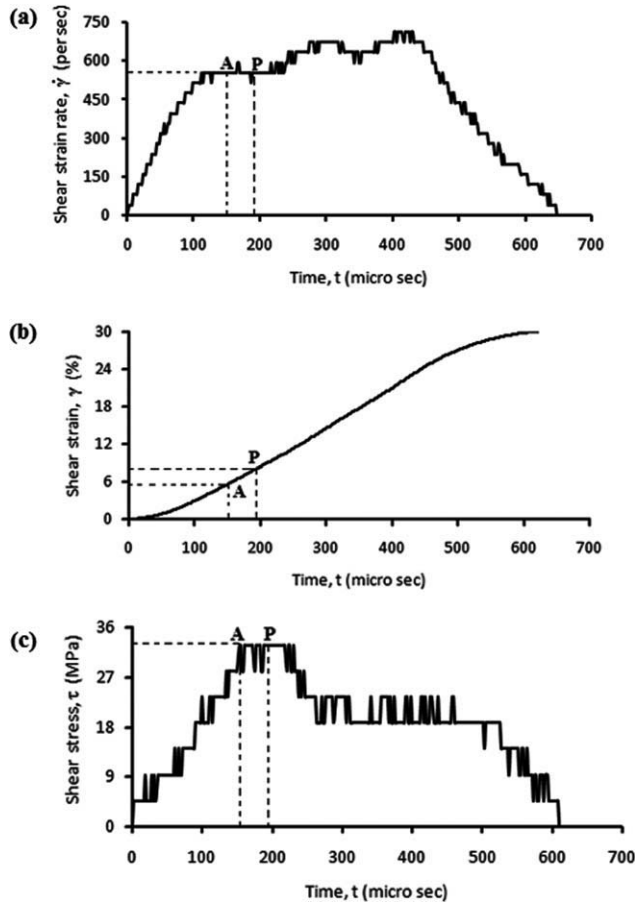

Figure 10 High strain rate shear test results for acrylic, $t_s = 2$ *mm*, $l_s = 2$ *mm*, $\dot{\gamma} = 553$ per sec: (a) shear strain rate versus time plot, (b) shear strain versus time plot, (c) shear stress versus time plot.

and macro damage formation, propagation, and fracture of the specimen take place. During the evolution of damage at the fracture surface, the shear stress wave that is transiting within the specimen would encounter the damages being formed. This would lead to incident pulse transmission and reflection at the fracture surfaces. Further, this would lead to stress wave attenuation. The stress at the interface between the incident bar and the specimen would be more than that at the interface between the transmitter bar and the specimen. In other words, the magnitude of $I + R$ would be more than the magnitude of T. Hence T_1 is more than T_2.

High strain rate shear test results are presented in Figures 10–12. Time versus shear strain rate plot, time versus shear strain plot and time versus shear stress plot are generated using the equations given in theory section and the strain gauge signals (Fig. 8). The results are presented in Figure 10. Here, point *P* indicates end of rise time and point A represents peak shear stress. For this case, shear strain rate is 553 per sec, shear strength is 31 MPa and the

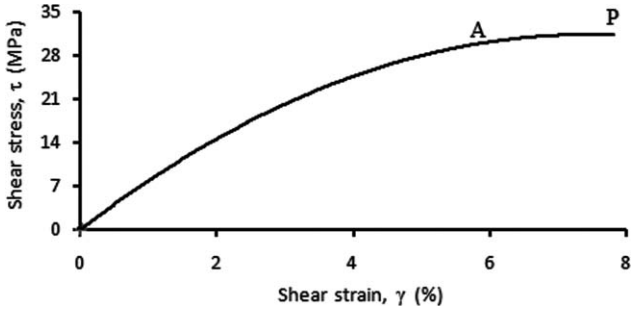

Figure 11 Shear stress versus shear strain plot for acrylic tested on TSHB apparatus, $t_s = 2$ *mm*, $l_s = 2$ *mm*, $\dot{\gamma} = 553$ per sec.

corresponding shear strain is 5.72%. The total duration of the incident pulse is about 570 μ s^{-1} and the rise time is about 190 μ s^{-1}. The fracture of the specimen takes place at time duration of 152 μ s^{-1}.

Time versus shear stress plot [Fig. 10(c)] can be subdivided into Regions I and II. Region I represents the behavior of the material until the shear strength is reached (up to Point A). Region II represents post failure behavior of the material (after Point A). The shear stress–shear strain plot as given in Figure 11 is generated using shear strain versus time and shear stress versus time plots as given in Figure 10. Point A in Figure 11 indicates the shear strength.

The shear strengths of acrylic under different strain rates are presented in Figure 12. The shear strength at quasi-static loading was estimated as 22 MPa. It can be observed that the shear strength is enhanced significantly at high strain rate loading compared with quasi-static loading. The shear strength enhancement at shear strain rate of 553 per sec is 25% compared with that at quasi-static loading. In the range shear strain rate considered there is an enhancement of shear strength from 25 to 28 MPa.

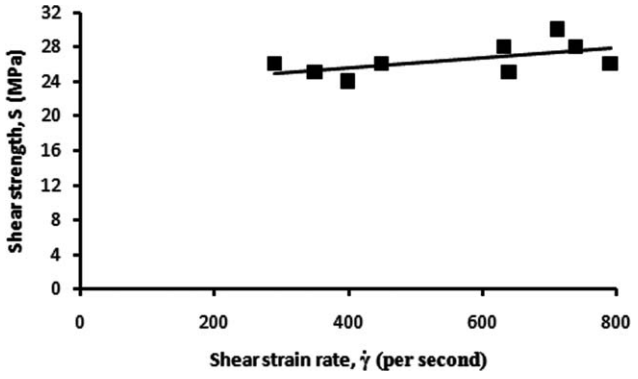

Figure 12 Shear strain rate versus shear strength plot obtained from test on TSHB apparatus, $t_s = 2$ *mm*, $l_s = 2$ *mm*, acrylic.

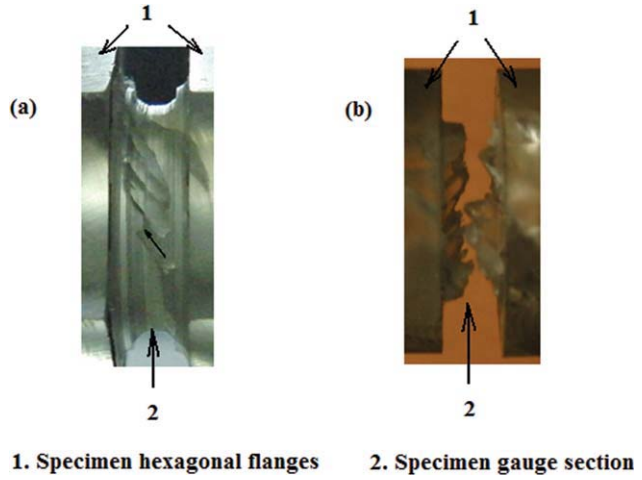

Figure 13 Photograph of failed specimens: (a) crack propagation along θ° to the axis of the specimen, (b) specimen broken into two pieces within the gauge length. [Color figure can be viewed in the online issue, which is available at wileyonlinelibrary.com.]

The qualitative behavior of epoxy studied by Gilat et al.[22–24] and Naik et al.[27] is similar to the observations of the present study for acrylic under high strain rate shear loading. The qualitative behavior obtained by the present study is also similar to the qualitative behavior obtained for plain weave E-glass/epoxy and plain weave carbon/epoxy.[26]

Photographs of failed specimens for acrylic under high strain rate shear loading are presented in Figure 13. Even though the cracks were confined to the gauge length, it was observed that multiple cracks had initiated at the shoulder of the specimen between the gauge length and the flanges. Further, macro cracks were observed at the gauge length following helical path along θ° to the axis of the specimen as shown in Figure 13(a). It was generally observed that the angle $\theta = 45°$. Specimen broken into two pieces within the gauge length after high strain rate shear loading is shown in Figure 13(b). The failure was in the gauge length. Multi-stage zigzag fracture was observed at the surfaces. Similar observation were made by Fleck et al.[19] and McCoy.[33]

Scanning electron microscope (SEM) images of the failed surfaces were studied. Figure 14(a) shows SEM image of acrylic failed at quasi static loading, and Figure 14(b) shows SEM image of acrylic tested at high strain rate loading. In both the cases multiple cracks were initiated forming multiple zigzag features. But formation of rougher surfaces with ridges, hackles and river patterns was observed on the specimen tested at high strain rate loading than that tested at quasi static loading. This can be due to rapid crack propagation that occurs at high strain rate loading.[33]

Generally, the shear strength is higher at high strain rate compared with that at quasi-static strain rate. This can be attributed to the fact that at lower strain rates the damage propagates slowly utilizing most of the applied energy. However, at higher strain rates, there is no sufficient time for the damage to initiate and propagate. Under such conditions, more work needs to be carried out for the damage initiation and propagation. This would lead to enhanced shear strength at high shear strain rates. The viscoelastic nature of the resin used is also responsible for the enhancement of shear strength.

CONCLUSIONS

Shear strengths of acrylic are generated under high strain rate loading. The experimental studies were carried out on a TSHB apparatus.

The failure was in the gauge length and multi-stage zigzag fracture was observed at the surfaces.

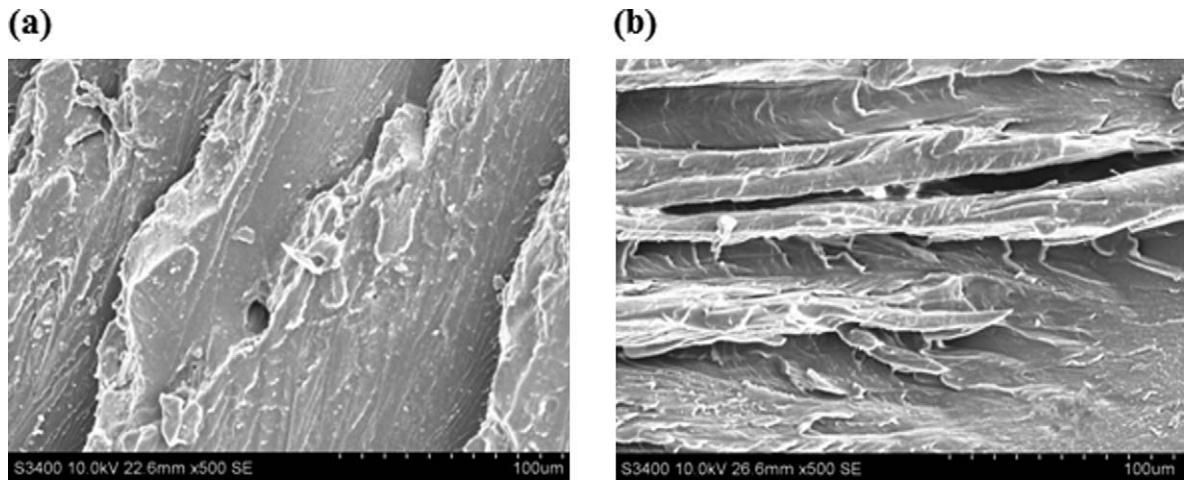

Figure 14 SEM images of failed surfaces for acrylic: (a) quasi-static shear loading, (b) high strain rate shear loading.

It was further observed that the shear strength is enhanced under high strain rate loading compared with quasi-static loading. The shear strength enhancement at shear strain rate of 553 per sec is 25% compared with that at quasi-static loading.

The qualitative behavior of acrylic is similar to those of different epoxies under high strain rate shear loading.

APPENDIX A

Torsional split Hopkinson bar apparatus

The photograph of the TSHB apparatus used for the studies is presented in Figure 1. The main components are: incident and transmitter elastic bars, torque pulley/rotary actuator, clamping mechanism, linear actuator, support blocks with rotary bearings and stand. The instruments used are: fatigue resistant strain gauges for dynamic measurement, balancing bridge, dynamic strain meter/amplifier, oscilloscope and computer. Incident and transmitter bars are made of aluminum alloy 6061-T6 with diameter of 25.4 mm and length of 1.9 m each.

The strain gauges on the incident bar are mounted in such a way that the distance between the strain gauges and the specimen is more than the distance between the clamp and the torque pulley. The strain gauges on the transmitter bar are mounted in such a way that the distance between the strain gauges and the specimen as well as the distance between strain gauges and rear end of the transmitter bar are more than the distance between the clamp and torque pulley. This ensures that overlap of pulses does not take place. Generally, the distance between the strain gauges on the incident bar and the specimen and the distance between the strain gauges on the transmitter bar and the specimen are the same.

Clamping mechanism is an important component of the apparatus. Photograph of the clamping mechanism is shown in Figure 2. The main components of clamping mechanism are: clamping vise, linear actuator and clamping bolt. Figure 2(a) shows the clamping arrangement before breaking the clamping bolt where as Figure 2(b) shows the clamping arrangement after breaking the clamping bolt. The details about clamping mechanism, clamping procedure and releasing the stored torque by breaking the clamping bolt are given in Refs. 26 and 27. As the clamping bolt breaks, the incident bar is unclamped instantaneously leading to release of stored torque. The clamping bolt material must exhibit minimum ductility, but must not be so brittle as to fracture before the clamp is tight enough to hold the desired torque. The notched clamping bolts were made using 6061-T6 and 2040-T6 aluminum alloys and EN24 steel.

APPENDIX B

Calibration

Calibration of TSHB apparatus was carried out by bonding together the incident and transmitter bars. With this the incident and transmitter bars together can be treated as a single bar. For bonding the incident and transmitter bars together, room temperature curing araldite adhesive was used. Strain gauge signals on oscilloscope during calibration are presented in Figure 5. Channel 1 shows the output of the strain gauge mounted on the incident bar whereas Channel 2 indicates the output of the strain gauge mounted on the transmitter bar. Here, I is the incident pulse with pulse duration equal to a_1a_2 whereas T is the transmitted pulse with pulse duration equal to b_1b_2. During calibration, reflected pulse (R) is not present. The magnitudes and durations of incident and transmitted pulses are nearly the same. The pulse durations a_1a_2 and b_1b_2 are equal $= 550\ \mu\ s^{-1}$.

Figure 6 presents comparison of torque versus time behavior derived from strain gauge signals during calibration on TSHB apparatus. Here, T_1 represents torque at the interface between the bars and calculated based on incident strain gauge signal I, whereas T_2 represents torque at the interface between the bars and calculated based on transmitted strain gauge signal T. From the figure it can be seen that torque versus time plots based on T_1 and T_2 are matching well. This indicates that the TSHB apparatus is perfectly aligned and friction free and ready for use for further experimentation. The torque induced is calculated as

$$T_1 = GJ/r(\gamma_I + \gamma_R) \tag{4}$$

$$T_2 = GJ/r(\gamma_T) \tag{5}$$

Here, G is shear modulus of the bars, J is polar moment of inertia of the bars, r is radius of the bars, γ_I is incident shear strain pulse, γ_T is transmitted shear strain pulse and γ_R is reflected shear strain pulse. During calibration, $\gamma_R = 0$.

References

1. Rosenberg, Z.; Surujon, Z.; Yeshurun, Y.; Ashuach, Y.; Dekel, E. Int J Imp Eng 2005, 31, 221.
2. Sierakowski, R. L.; Chaturvedi, S. K. Dynamic Loading and Characterization of Fiber-Reinforced Composites; Wiley-Interscience Publication: New York, 1997; p15.
3. Sayers, K. H.; Harris, B. J Compos Mater 1973, 7, 129.
4. Werner, S. M.; Dharan, C. K. H. J Compos Mater 1987, 20, 365.
5. Harding, J.; Li, Y. L. Compos Sci Tech 1992, 45, 161.
6. Harding, J.; Dong, L. Compos Sci Tech 1994, 51, 347.
7. Bouette, B.; Cazenuve, C.; Oytana, C. Compos Sci Tech 1992, 45, 313.

8. Dong, L.; Harding, J. Compos 1994, 25, 129.
9. Hallett, S. R.; Ruiz, C.; Harding, J. Compos Sci Tech 1999, 59, 749.
10. Bing, Q.; Sun, C. T. Compos Sci Tech 2005, 65, 2481.
11. Duffy, J.; Campbell, J. D.; Hawley, R. H. J Appl Mech 1971, 38, 83.
12. Leung, E. K. J Appl Mech 1980, 47, 278.
13. Hartley, K. A.; Duffy, J.; Hawley, R. W. The Torsional Kolsky (Split-Hopkinson) Bar; ASM Metals Handbook, Materials Park: Ohio, 1985; Vol. 8, p 218.
14. Leber, H.; Lifshitz, J. M. Compos Sci Tech 1996, 56, 391.
15. Lifshitz, J. M.; Leber, H. Compos Sci Tech 1998, 58, 987.
16. Gillespie, J. W., Jr.; Gama, B. A.; Cichanowski, C. E.; Xiao, J. R. Compos Sci Tech 2005, 65, 1891.
17. Dai, L. H.; Bai, Y. L.; Lee, S. W. R. Compos Sci Tech 1998, 58, 1667.
18. Dai, L. H.; Bai, Y. L.; Lee, S. W. R. Key Eng Mater 1998, 141–143, 651.
19. Fleck, N. A.; Stronge, W. J.; Liu, J. H. Proc R Soc Lond A Mater 1990, 429, 459.
20. Jelf, P. M.; Fleck, N. A. J Mater Sci 1994, 29, 3080.
21. Hu, Y.; Feng, R. J Appl Mech 2004, 71, 441.
22. Gilat, A.; Goldberg, R. K.; Roberts, G. D. J Phys IV 2003, 110, 123.
23. Gilat, A.; Goldberg, R. K.; Roberts, G. D. Strain Rate Sensitivity of Epoxy Resin in Tensile and Shear Loading; NASA/TM-213595, NASA Center for Aerospace Information: Hanover, MD, 2005.
24. Gilat, A.; Goldberg, R. K.; Roberts, G. D. J Aerospace Eng 2007, 20, 75.
25. Hou, J. P.; Ruiz, C.; Trojanowski, A. Mater Sci Eng A 2000, 283, 181.
26. Naik, N. K.; Addis, A.; Kavala, V. R.; Veerraju, Ch. Mech Mater 2007, 39, 1043.
27. Naik, N. K.; Ravikumar, G.; Thoram, N. M.; Kavala, V. R.; Veerraju, C. Polym Eng Sci 2010, 50, 780.
28. Jacob, G. C.; Starbuck, J. M.; Fellers, J. F.; Simunovic, S.; Boeman, G. R. J Apply Polym Sci 2004, 94, 296.
29. Odeshi, A. G.; Owolabi, G. M.; Singh, M. N. K.; Bassim, M. N. Metall Mater Trans A 2007, 38A, 2674.
30. Marchand, A.; Duffy, J. J Mech Phys Solids 1988, 36, 251.
31. Cepus, E.; Liu, C. D.; Bassim, M. N. J Phys 1994, 4, 3.
32. Bassim, M. N.; Panic, N. J Mater Proc Tech 1999, 92/93, 481.
33. McCoy, R. A. J Fail Anal Prev 2004, 4, 58.